Insight into sodium silicate glass structural organization by multinuclear NMR combined with first-principles calculations

Frédéric Angeli, Olivier Villain, Sophie Schuller, Simona Ispas, Thibault Charpentier

Insight into sodium silicate glass structural organization by multinuclear NMR combined with first-principles calculations

Frédéric Angeli [a,*], Olivier Villain [b], Sophie Schuller [c], Simona Ispas [d], Thibault Charpentier [b,*]

[a] CEA, DEN, Laboratoire d'étude du Comportement à Long Terme, 30207 Bagnols-sur-Cèze, France
[b] CEA, IRAMIS, Laboratoire de Structure et Dynamique par Résonance Magnétique, UMR CEA/CNRS 3299 91191 Gif-sur-Yvette, France
[c] CEA, DEN, Laboratoire d'étude et Développement des Matrices de conditionnement, 30207 Bagnols-sur-Cèze, France
[d] Université Montpellier 2, CNRS, Laboratoire Charles Coulomb UMR 5221, F-34095, Montpellier, France

Received 6 August 2010; accepted in revised form 3 February 2011

Abstract

Short and medium range order of silica and sodium silicate glasses have been investigated from a quantitative analysis of ^{29}Si MAS NMR and ^{23}Na, ^{17}O MQMAS NMR spectra. The method described enables the extraction of the underlying ^{17}O NMR parameter distributions of bridging oxygens (BOs) and non-bridging oxygens (NBOs), and yields site populations which are confirmed by ^{29}Si NMR data. The extracted NMR parameter distributions and their variations with respect to the glass chemical composition can then be analyzed in terms of local structural features (bond angles and bond lengths, coordination numbers) with the help of molecular dynamics simulations combined with first-principles calculations of NMR parameters. Correlations of relevant structural parameters with ^{23}Na, ^{29}Si and ^{17}O NMR interactions (isotropic chemical shift δ_{iso}, quadrupolar coupling constant C_Q and quadrupolar asymmetry parameter η_Q) are re-examined and their applicability is discussed. These data offer better insights into the structural organization of the glass network, including both chemical and topological disorder. Adding sodium to pure silica significantly diminishes the Si–O–Si bond angles and leads to a longer mean Si–O bond length with a slight decrease of the mean Na–O bond length. Moreover, the present data are in favor of a homogeneous distribution of Na around both oxygen species in the silicate network. Finally, our approach was found to be sensitive enough to investigate the effect of addition of a small quantity of molybdenum oxide (about 1 mol%) on the ^{17}O MAS spectrum, opening new possibilities for investigating the Mo environment in silicate glasses.

1. INTRODUCTION

Silica and binary sodium silicate oxide glasses are the main constituent of numerous industrial and natural glasses, and represent important simplified model systems for assessing new approaches for structural investigations. However, their short and medium-range structural disorder is still debated and remains difficult to evaluate; even for vitreous silica, the quantification of structural disorder, mainly related to the distribution of Si–O–Si bond angles and Si–O bond lengths, can only be obtained from the interpretation of experimental data such as diffraction experiments (Neuefeind and Liss, 1996), nuclear magnetic resonance (NMR) spectroscopy (Farnan et al., 1992; Clark et al., 2004; Charpentier et al., 2009) or theoretically by molecular dynamics (MD) simulations (Yuan and Cormack, 2003; Carré et al., 2008; Giacomazzi et al., 2009).

The addition of network modifier atoms to silica adds a supplementary level of complexity. Although the effect of alkali cations on depolymerization of the glass network is clearly established (Schneider et al., 1987; Emerson et al., 1989; Maekawa et al., 1991), it is uncertain whether the

* Corresponding authors. Tel.: +33 4 66 79 1876 (F. Angeli), +33 1 69 08 2356 (T. Charpentier).
E-mail addresses: frederic.angeli@cea.fr (F. Angeli), thibault.charpentier@cea.fr (T. Charpentier).

alkalis are randomly distributed (Zachariasen, 1932) or concentrated into areas rich in nonbridging oxygen atoms (NBO), leaving regions rich in silica (Greaves, 1985, 1989; Gaskell et al., 1991; Henderson, 1995; Meyer et al., 2004; Kargl et al., 2006). MD simulations have suggested a distribution of sodium slightly more clustered than a random distribution with the formation of sodium rich channels (Horbach et al., 2002; Du and Cormack, 2004; Meyer et al., 2004).

The influence of the Na/Si ratio in binary sodium silicate glass was recently experimentally investigated by ^{17}O MQMAS NMR (Lee and Stebbins, 2009). For compositions containing up to 50 mol% Na_2O, the quadrupolar coupling parameters of all oxygen species (i.e., BO and NBO sites) were a function of sodium content, leading to the conclusion that the investigated glass compositions do not consist of separated regions rich in sodium or silicon: changes in both BOs and NBOs were induced by addition of sodium, and not only NBOs as generally assumed by the modified random-network model (Greaves, 1985, 1989; Gaskell et al., 1991). Although these data provide valuable qualitative results for a discussion of glass structural models, more detailed interpretation would have been possible if a quantitative processing scheme could have been used to extract the site population, allowing the reconstruction of NMR parameter distributions of each observed site.

The combination of experimental data with atomic scale calculations is a complementary quantitative approach. ^{29}Si magic-angle spinning (MAS) NMR and ^{17}O multiple quantum (MQ)MAS NMR have been successfully used to extract structural data from the interpretation of NMR parameters (isotropic chemical shift δ_{iso}, quadrupolar coupling constant C_Q and quadrupolar asymmetry parameter η_Q) such as bond lengths and bond angles (Pettifer et al., 1988; Farnan et al., 1992; Mauri et al., 2000; Clark and Grandinetti, 2003, 2005). Such correlations were extensively investigated (Clark and Grandinetti, 2003; Clark et al., 2004) with relationships between the Si–O–Si angle, Si–O distance and ^{17}O quadrupolar coupling parameters (C_q and η_Q) established from ab initio calculations (Clark and Grandinetti, 2005). However, such studies were carried out using clusters to model the oxygen atom environment, a finite-size approach that does not take into account the inherent medium and long range structural constraints of the vitreous state, which is the primary aim of MD simulations.

With the introduction of the Density Functional Theory (DFT) Gauge Including Projector Augmented Wave (GIPAW) method (Pickard and Mauri, 2001), large systems (with typically a few hundred atoms) can now be used to accurately calculate the NMR parameters in amorphous materials (Charpentier et al., 2004). Combination of GIPAW calculations with MD simulations have opened new routes for interpreting NMR parameter distributions, refining relationships between NMR parameters and local structural features (Charpentier et al., 2009; Ispas et al., 2010) or more simply for analyzing NMR data of complex materials (Soleilhavoup et al., 2010; Pedone et al., 2010a; Forler et al., 2010).

Table 1
Analyzed molar composition of ^{17}O enriched glasses.

Glass	SiO_2 (mol%)	Na_2O (mol%)	MoO_3 (mol%)
SiO_2	100	–	–
NS3	77.5	22.5	–
NSMo	59.4	39.8	0.8
NS1	56.9	43.1	–

In the present work, we apply this approach to obtain quantitative structural data from the analysis of ^{29}Si, ^{23}Na and ^{17}O NMR spectra. We describe the acquisition of structural parameters from ^{23}Na and ^{29}Si MAS NMR and the quantitative reconstruction of the three-dimensional NMR parameter distributions (C_Q, η_Q, δ_{iso}) for each oxygen species from ^{17}O MQMAS spectra, taking into account the effects of correlations between NMR parameters as recently described for vitreous silica (Charpentier et al., 2009). These data can then be used as a basis for discussion of alkali distribution in the glass network. MD simulations and first-principles calculations of NMR parameters are used in support of the qualitative or quantitative interpretation of the experimental NMR data.

First of all, silica glass serves as a reference composition. The influence of sodium content in the silicate network is then examined. Consideration of sodosilicate glasses is completed by a ternary glass containing a small amount of molybdenum (less than 1 mol%) to get an insight into its signature in sodium silicate glasses. Understanding the influence of molybdenum on glass structure is a major issue for numerous applications (Farges et al., 2006). Molybdenum can affect the medium-range disorder to the extent that it increases network polymerization as network-modifying cations become $[MoO_4]^{2-}$ charge compensators (Calas et al., 2003; Short et al., 2005; Farges et al., 2006; Caurant et al., 2007, 2010). Molybdenum is found in small quantities in high-level nuclear waste containment glass matrices (Advocat et al., 2001), where it can form alkali molybdate crystals leading to phases of low chemical durability (Pinet et al., 2006). Its interaction with the silicate network must be determined to control its solubilization in the matrix, thereby optimizing its concentration and avoiding phase separation. ^{95}Mo MAS NMR provides additional data on the local environment of molybdenum through direct study (Kroeker et al., 2009), but a more comprehensive overview can be obtained by using ^{17}O NMR data, notably by highlighting the structural changes induced by molybdenum.

2. EXPERIMENTAL CONDITIONS

2.1. Fabrication of glasses enriched in ^{17}O

The materials were synthesized by the sol–gel process, involving hydrolysis (40% enriched water) and polycondensation from metal alkoxides. All the elements were used in alkoxide form ($Si(OC_2H_5)_4$, $Na(OC_2H_5)$) and mixed together in anhydrous ethanol. The metal precursors used for glass fabrication were enriched according to the following reactions:

$$M(O-R)_n + H_2{}^{17}O \rightarrow M(O-R)n - 1^{17}OH + R{-}OH$$
$$M(O-R)_{n-1} - {}^{17}OH + M'(O-R)_{n-1} - {}^{17}OH \rightarrow (O-R)_{n-1})M - {}^{17}O - M'(O-R')_{n-1} + H_2O$$

where M and M′ are cations; R and R′ are organic groups.

The quantity of $H_2{}^{17}O$ added was the exact stoichiometry according to the first reaction. The resulting precursors were melted for 30 min on platinum foil at 1200 °C. The glass was analyzed by alkaline fusion ($NaOH + KNO_3$ and $Li_2B_4O_7$,$5H_2O$) of powder samples (~50 mg) then dissolved in HNO_3 for ICP-AES analysis. The analyzed glasses chemical composition is indicated in Table 1.

It is of note that Mo species are not crystallized in the NSMo glass; despite the fact that detection of small amounts (typically <1%) of crystalline phase is difficult by XRD, NMR offers a much more sensitive approach, with which even lower quantities of crystalline Na_2MoO_4 would have been easily detected in the present sample from ^{23}Na MAS NMR. A crystalline reference material of this phase has been synthesized using ^{17}O.

2.2. MAS and MQMAS NMR

Experimental spectra were acquired with a Bruker 500WB spectrometer (magnetic field strength 11.72 T) with a 4 mm CPMAS probe. The rotation frequency was 12.5 kHz for all the experiments. A 1 s recycle delay and a short 1 μs pulse length were used to obtain quantitative spectra for ^{23}Na. ^{29}Si spectra were obtained using a CPMG pulse sequence (Larsen and Farnan, 2002) and a 200 s recycle delay. ^{17}O MQMAS spectra were obtained using a Z-filter pulse sequence with the parameters indicated in (Angeli et al., 2008) and a 1 s recycle delay for all the samples except SiO_2 (4 s). The spectra were processed with home-built software. ^{29}Si spectra were referenced to an external TKS sample for which the highest-intensity peak is situated at −9.9 ppm from that of TMS. For ^{17}O and ^{23}Na external frequency references were H_2O and 1 M NaCl solution, respectively.

For ^{23}Na, MQMAS and MAS spectra were fitted as described in (Angeli et al., 2007) using NMR parameter distributions accounting for the underlying structural disorder as the product:

$$\pi(C_Q, \eta_Q, \delta_{iso}) = G(\delta_{iso}; \bar{\delta}_{iso}, \sigma_{iso}) \times P(C_Q, \eta_Q; \sigma_Q) \quad (1)$$

The Normal (Gaussian) distribution $G(\delta_{iso}; \bar{\delta}_{iso}, \sigma_{iso})$ with the mean value $\bar{\delta}_{iso}$ and standard deviation σ_{iso} accounts for the distribution of δ_{iso}:

$$G(\delta_{iso}; \bar{\delta}_{iso}, \sigma_{iso}) = \frac{1}{\sqrt{2\pi}\sigma_{iso}} \exp\left\{-\frac{(\delta_{iso} - \bar{\delta}_{iso})^2}{2\sigma_{iso}^2}\right\}$$

$P(C_Q, \eta_Q; \sigma_Q)$ is the Gaussian Isotropic Model (GIM) accounting for the distribution of the electric field gradient (here characterized by C_Q and η_Q) (Czjzek et al., 1981; Neuville et al., 2004):

$$P(C_Q, \eta_Q; \sigma_Q) = \frac{1}{\sqrt{2\pi}\sigma_Q^5} C_Q^4 \eta_Q \left(1 - \frac{\eta_Q^2}{9}\right) \times \exp\left\{-\frac{C_Q^2(1 + \eta_Q^2/3)}{2\sigma_Q^2}\right\}$$

For each sample, the fit of MAS and MQMAS spectra yielded the three parameters $\bar{\delta}_{iso}$ σ_{iso} and σ_Q which determine the distribution (Eq(1)). From the latter, mean and standard deviation values of each NMR parameter C_Q, η_Q and δ_{iso} were calculated, reported in Table 3.

For ^{17}O, it was necessary to introduce a NMR parameter distribution model that accounts for correlation effects between the NMR parameters $(C_Q, \eta_Q, \delta_{iso})$, as initially found experimentally for vitreous silica (Clark et al., 2004) then latter corroborated by first-principles calculations (Charpentier et al., 2009). Such correlations were also observed for our data (see text) and accordingly, the following 3D NMR parameter distributions was used:

$$p(C_Q, \eta, \delta_{iso}) = G(C_Q - \overline{C_Q}; \sigma_C) \times G(\eta - f_\eta(C_Q); \sigma_\eta) \times G(\delta_{iso} - f_\delta(C_Q); \sigma_\delta) \quad (2)$$

where G is a Gaussian distribution with standard deviation. The functions f represent the constraint of linear correlated variation between the NMR parameters as follows:

$$f_x(C_Q) = a_x C_Q + b_x \quad (3)$$

for $x = \eta$ and δ.

^{17}O MQMAS data were fitted taking into account these NMR parameter distribution effects as well as the influence of the pulse sequence and sample spinning which turn out to be crucial for accurate quantification of each site population (Angeli et al., 2008). As done for ^{23}Na, once the parameters of the distribution were determined (here, a_η, b_η, a_δ, b_δ, σ_η, σ_δ, σ_C and $\bar{C}_Q$), the mean and standard deviation values of each NMR parameter were calculated.

In every case (^{29}Si, ^{23}Na, ^{17}O), errors of the reported values were estimated as follows. Each parameter was varied independently so as to increase the error χ^2 by a factor 2, and the range of variation of the reported parameters (i.e. the mean and standard deviation values and the intensity of each line) provided an estimate of their accuracy.

Table 2
Glass compositions and cell parameters used for molecular dynamics simulations and DFT geometry optimization.

Glass	Size	Composition	Cell side (Å)[a]	DFT Volume (Å^3)[b]
N40S60	240	$Na_{64}Si_{48}O_{128}$	14.724	3077.3
N23S77	300	$Na_{46}Si_{77}O_{177}$	16.096	3887.0
N45S55	300	$Na_{90}Si_{55}O_{155}$	15.832	3745.5

[a] (Cubic) cell side for the classical MD simulations.
[b] Unit cell volume after the DFT geometry optimization.

3. MOLECULAR DYNAMICS SIMULATIONS AND GIPAW NMR CALCULATIONS

In order to provide support for the qualitative and quantitative interpretation of the present experimental NMR data, sodium silicate glass models were generated within a combined classical MD and first-principles calculations framework as previously described (Ispas et al., 2010). For the classical MD simulations, empirical pairwise potentials based on a rigid ionic model as parameterized by (Pedone et al., 2006) were employed. The velocity Verlet algorithm as encoded in the DL_POLY package (Smith and Forester, 1996) was used to integrate the equations of motion, with a time-step of 0.5 fs and periodic boundary conditions. Coulombic interactions were calculated by the Ewald summation method with a cutoff radius of half the edge length of the simulation box (see below) and an accuracy of 10^{-5}.

Liquid models were prepared by inserting Na_2O and SiO_2 units in a cubic box according to the glass composition and the experimental glass density, with parameters given in Table 2. The systems were initially equilibrated at 6000 K for 20 ps in the NVT ensemble to ensure suitable mixing of the melt and then cooled down to 3500 K using a quenching rate of 10^2 K/ps. The systems were then equilibrated at this temperature for 250 ps in the NVT ensemble, and a subsequent run of 250 ps was performed in the NVE ensemble. Liquids were then cooled to 300 K at a nominal cooling rate of 0.2 K/ps followed by a final NVE trajectory of 100 ps.

Before computing the NMR parameters, geometry optimization with variable unit cell volume of the above classical glass model was performed within the DFT framework using the GGA-PBE functional (Perdew et al., 1996) as implemented in the PWSCF code (Giannozzi, 2009). A single Baldereschi k-point and a plane-wave basis up to an energy cutoff of 60 Ry were used, while core electrons were replaced by ultrasoft atomic pseudopotentials from the Quantum Espresso library (Giannozzi, 2009). In order to *calibrate* the deviation of the predicted equilibrium volume from its experimental value, the geometry of reference crystalline sodium silicate compounds was also optimized (Na_2SiO_2, α-$Na_2Si_2O_5$ and β-$Na_2Si_2O_5$). Forces and bulk modulus were relaxed to values smaller than 0.001 Ry/a.u. (0.026 eV/Å) and 0.01 GPa using different Monkhorst-Pack k-point grids ($4 \times 4 \times 4$, $2 \times 2 \times 4$ and $2 \times 2 \times 2$, respectively). For all compounds, an overestimation of the experimental equilibrium volume of about 4.5%

Table 3
NMR parameters of sites of each nucleus obtained by fitting the ^{23}Na MAS, ^{29}Si MAS and ^{17}O MQMAS data shown in Figs. 1 and 5 (standard deviations are indicated in parentheses, see text). Mean Na–O bond lengths are calculated from mean ^{23}Na δ_{iso} and mean Si–O bond lengths from ^{17}O δ_{iso} with MD-GIPAW correlations and previous relationships obtained on crystalline compounds (see Fig. 3 and Fig. 8). The proportion of $Q^{(n)}$ species is obtained from the simulated ^{29}Si MAS spectra. The NBO proportion is deduced from these data and compared with direct ^{17}O NMR measurement.

	Site	Parameters	NS1	NSMo	NS3	SiO_2
^{23}Na		$\delta_{iso}(ppm) - (\sigma_{\delta_{iso}})$	7.5 (9.4)	6.2 (9.5)	2.7 (9.4)	
		$C_Q(MHz) - (\sigma_{C_Q})$	3.0 (2.3)	3.1 (2.4)	3.5 (2.7)	
		$d(Na-O)$(Å)[a]	2.54 (0.05)	2.55 (0.05)	2.57 (0.05)	
		$d(Na-O)$(Å)[b]	2.50 (0.11)	2.52 (0.11)	2.56 (0.11)	
^{29}Si	Q^2	$\delta_{iso}(ppm) - (\sigma_{\delta_{iso}})$	−76.0 (4.4)	−76.9 (4.3)	−75.0 (6.0)	
	Q^3		−85.2 (3.0)	−86.2 (2.9)	−91.1 (4.4)	
	Q^4				−104.0 (5.7)	−110.7 (4.5)
	Q^2	Proportion (%)	55.0	24.0	2.3	0
	Q^3		45.0	76.0	60.5	0
	Q^4		0	0	37.2	100
		NBO (%)	56	47	28	
^{17}O	Si–O–Si	$\delta_{iso}(ppm) - (\sigma_{\delta_{iso}})$	61.9 (4.5)	59.3 (4.6)	49.8 (6.8)	36.7 (4.7)
		$C_Q(MHz) - (\sigma_{C_Q})$	4.4 (0.2)	4.4 (0.2)	4.8 (0.3)	5.3 (0.3)
		$\eta_Q - (\sigma_{\eta_Q})$	0.5 (0.2)	0.4 (0.1)	0.4 (0.2)	0.15 (0.1)
		$d(Si-O)$(Å)[c]	1.645 (0.008)	1.640 (0.008)	1.623 (0.012)	1.600 (0.008)
		$d(Si-O)$(Å)[d]	1.645 (0.011)	1.638 (0.012)	1.614 (0.017)	1.582 (0.012)
	Si–O–Na	$\delta_{iso}(ppm) - (\sigma_{\delta_{iso}})$	41.0 (4.6)	39.5 (4.9)	36.0 (5.6)	
		$C_Q(MHz) - (\sigma_{C_Q})$	2.1 (0.3)	2.1 (0.3)	2.1 (0.3)	
		$\eta_Q - (\sigma_{\eta_Q})$	0.7 (0.1)	0.7 (0.1)	0.7 (0.1)	
		NBO (%)	58	47	26	

Note: ^{23}Na. precision C_Q: 0.15 MHz, δ_{iso}: 1 ppm (for both mean and standard deviation values), ^{29}Si. precision δ_{iso}: 0.3 ppm, ^{17}O. precision C_Q: 0.25 MHz, δ_{iso}: 2 ppm.

[a] Na–O bond length extracted from present MD-GIPAW calculations: $d(Na–O) = -0.0054\delta_{iso}(^{23}Na) + 2.5835$.

[b] Na–O bond length from previous correlation on crystalline silicates: $d(Na–O) = -0.0119\delta_{iso}(^{23}Na) + 2.5912$ (Angeli et al., 2000a and references therein).

[c] Si–O bond length extracted from present MD-GIPAW calculations: $d(Si–O) = 0.00176\delta_{iso}(^{17}O) + 1.5357$.

[d] Si–O bond length from previous correlation on crystalline silicates: $d(Si–O) = 0.0025\delta_{iso}(^{17}O) + 1.4898$ (Ashbrook et al., 2002 and references therein).

was observed. Accordingly, before performing NMR calculations, the unit cell volume of the glass model was rescaled by 4.5%, as done in previous works (Charpentier et al., 2009; Ispas et al., 2010).

DFT NMR calculations were carried out with the CASTEP code (Segall et al., 2002; Clark et al., 2005) using the GIPAW method (Pickard and Mauri, 2001; Profeta et al., 2003; Yates et al., 2007) and a single Baldereschi point. Employed ultra-soft pseudopotentials have been described in (Pedone et al., 2010b). GIPAW outputs were processed using the fpNMR platform (Charpentier et al., 2009; Pedone et al., 2010b), in order to correlate the computed NMR parameters for each atomic species (hereafter referred to as MD-GIPAW) to local structural features (coordination number, bond angles and bond lengths).

4. RESULTS AND DISCUSSION

The interpretation of NMR parameters is presented in this section from ^{23}Na, ^{29}Si and ^{17}O NMR data. The previous empirical relationships between ^{23}Na (^{17}O) δ_{iso} and Na–O(Si–O, respectively) bond lengths are compared with the MD-GIPAW calculations. ^{29}Si and ^{17}O spectra are used to visualize the effects of Mo incorporation on the binary glass structure. Then, the approach used to extract the NMR parameters of ^{29}Si and ^{17}O in order to determine bond angles is addressed. From these data, correlations between bond angles (Si–O–Si) and bond lengths (Si–O and Na–O), as well as the distribution of alkali ions in the glass network are discussed.

4.1. Sodium-23 NMR

The experimental and simulated ^{23}Na MAS NMR spectra are shown in Fig. 1a, while the NMR parameters (δ_{iso} and C_Q) are indicated in Table 3. As illustrated in Fig. 2, for each sample ^{23}Na MQMAS NMR data have first been fitted to constrain the NMR parameter distributions (see Experimental section). The latter were then used to fit the MAS spectra with tolerance of a small variation (typically 5–10%) of its parameters. This approach has allowed us to obtain more information (i.e. mean and standard deviation values) than the determination of the center of gravity of spectra (more specifically of the central band) collected at multiple fields (Gee et al., 1997). Furthermore, such determinations can be very tricky because of the overlap (even small) between the spinning sidebands and the central band as a result of the finite sample spinning frequency.

Increasing the sodium content in the glass results in an increase in δ_{iso} and a slight decrease in C_Q. Numerous chemical and geometrical parameters can influence these NMR interactions. It has been observed from crystalline materials that longer Na–O bond distances, higher coordination number and lower NBO resulted in greater electronic shielding and consequently a more negative (lower frequency) δ_{iso} for sodium (Xue and Stebbins, 1993; George and Stebbins, 1995; Maekawa et al., 1997; Stebbins, 1998). Determining the δ_{iso} values by ^{23}Na MQMAS NMR allowed the extraction of a correlation between the glass chemical composition and the Na–O bond length in sodium silicate glasses (Angeli et al., 1999, 2000a; Lee and Stebbins, 2003).

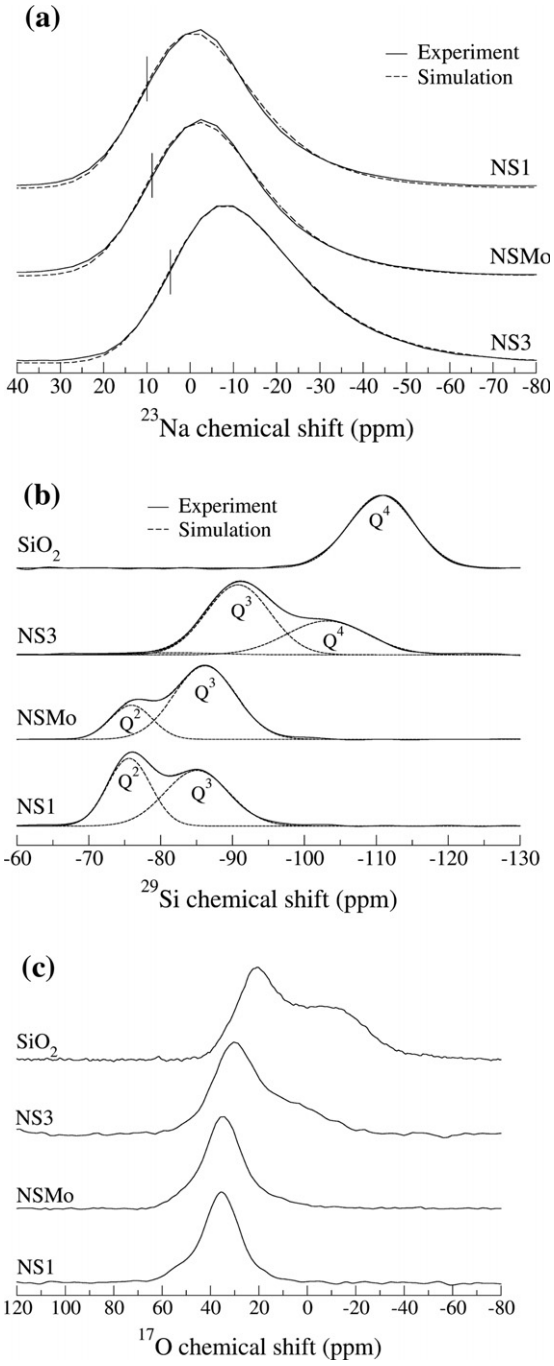

Fig. 1. Experimental (solid lines) and simulated (peak fitting, dashed lines) ^{23}Na (a), ^{29}Si (b) and ^{17}O (c) (not simulated because ^{17}O MQMAS was used) MAS NMR spectra. Isotropic chemical shift of ^{23}Na is indicated by solid verticals lines.

The Na–O bond length estimated for our glass samples are reported in the Table 3, first using a previous relationship coming from crystalline silicate materials (d(Na–O) = $-0.0119.\delta_{iso} + 2.5912$) (Angeli et al., 2000a and references therein) and secondly from a correlation obtained

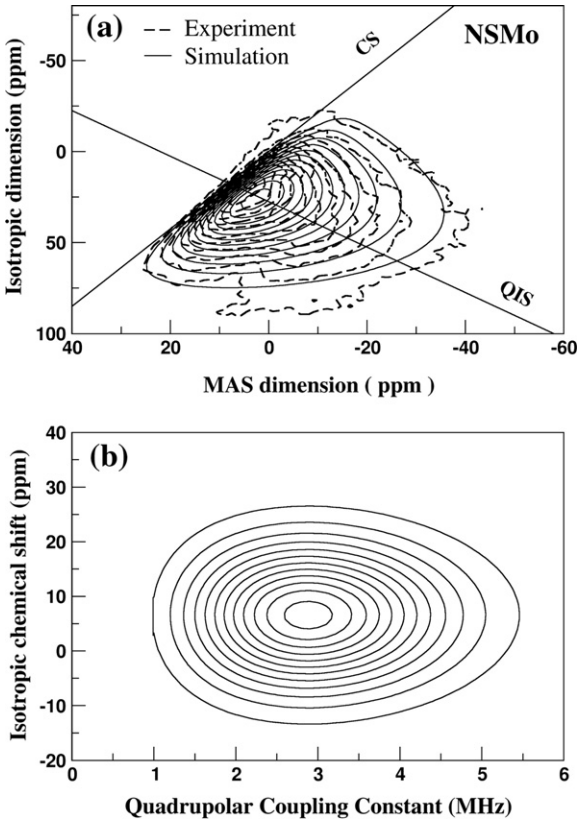

Fig. 2. (a) Fitted simulation (solid lines) and experimental (dashed lines) ^{23}Na MQMAS spectrum of the NSMo sample. The CS and QIS lines represent the direction of broadening as induced by isotropic chemical shift distribution or quadrupolar distribution (Quadrupolar Induced Shift). (b) NMR parameter distribution (here projected on the C_Q, δ_{iso} space) used for the MQMAS and MAS simulations.

from MD-GIPAW data plotted in Fig. 3 ($d(Na–O) = -0.0054.\delta_{iso} + 2.5835$, see more details below). The MD-GIPAW approach gives a slightly higher Na–O bond distance. The data thus show that increasing the Na_2O content from 23% to 46% is responsible for only a low decrease in the mean Na–O bond distance between 0.03 Å (MD-GIPAW approach) and 0.06 Å (empirical relationship). It is important to remark that the values (2.50–2.57 Å) extracted in the present work seems higher than those recently reported from neutron and X-ray diffraction data, equal to 2.29 Å and defined as radial distribution function (RDF) peak maximum (Fabian et al., 2007). At this stage, it is worth noticing that our mean ⟨Na–O⟩ distance corresponds to an average value over a sphere of radius r_c (here equal to 3.2 Å) around each sodium atom.

$$\langle \mathrm{Na-O} \rangle_{NMR} = \frac{\int_0^{r_c} r g_{\mathrm{NaO}}(r) dr}{\int_0^{r_c} g_{\mathrm{NaO}}(r) dr} \quad (4)$$

Our MD data yielded RDF peak maximum between 2.25 and 2.30 Å, and mean Na–O distance between 2.44 and 2.45 Å. Thus our estimation compares very well with the experimental data, despite a slight overestimation of about 0.1 Å .

We have also noticed both a decrease of δ_{iso} and an increase of the mean Na–O distance for increasing oxygen coordination number as seen in Table 4. The observed slight overestimation by MD-GIPAW of C_Q (see comparison with Table 3) may be attributed to thermal effects (motions and vibrations) which are not yet incorporated in the present calculations. Indeed, these calculations were performed at 0 K and vibrational calculations are required to incorporate finite temperature effects into the NMR parameters (Rossano et al., 2005).

We have then considered the shortest Na–BO and Na–NBO bond lengths present in the MD glass models as indicators of the interaction of Na with bridging and non-bridging oxygen (Table 4). Both bond lengths are modified by the oxygen coordination. This suggests that sodium cations have in their local environment both NBOs and BOs, and they do not appear to be surrounded by NBOs in alkali rich regions. The more oxygen atoms that are present in the Na environment, the more Na is found closer to the BOs to the detriment of the increase of Na–NBO bond distance. The shorter mean Na–O distances with added sodium content (Table 3) are thus probably related to the increase of NBO coordination around sodium due to the shorter bond lengths of Na–NBO compared to Na–BO.

4.2. Silicon-29 NMR

Fig. 1b clearly shows the strong increase in the ^{29}Si δ_{iso} with added Na, indicating network depolymerization as first reported in the nineties (Schneider et al., 1987; Emerson et al., 1989; Maekawa et al., 1991; Engelhardt and Koller, 1994). The quantification of Q^n species (where $n = 0$ to 4 refers to the number of bridging oxygen atoms) based on the simulated ^{29}Si spectra is indicated in Table 3. Only the glass NS3 with the lowest alkali content (23% Na_2O) contains a significant fully polymerized network fraction (37% Q^4), while the most depolymerized glass (NS1) contains mainly Q^2 species (55%). These values are well correlated with glass composition, assuming that a sodium atom produces one NBO atom in binary sodium silicate glasses; the average chemical composition computed from the ^{29}Si and ^{17}O data (NBO) indicates 24% Na_2O for NS3 (compared to 23%) and 44% for NS1 (compared to 43%). They are equally supported by ^{17}O MQMAS NMR analyse: the number of NBO calculated from the proportion of Q^n species is compared with the direct ^{17}O NMR measurement in Table 3, and the two values agree to within 2%.

4.2.1. Molybdenum incorporation

In an ideal case, we would like to compare two ^{17}O enriched glass samples, with and without molybdenum, having strictly identical Si/Na ratios, but this is very difficult to obtain. Nevertheless, with the present data we can discuss the effect of molybdenum on the glass structure by comparing the difference between NBO proportion in the Mo-bearing glass and the calculated value without taking Mo into account. Hence the calculated NBOs for the latter (50%) should be near the actual value considering the close agreement experimentally obtained for the other binary glasses (i.e. the NS1 and NS3 compositions). The NBO

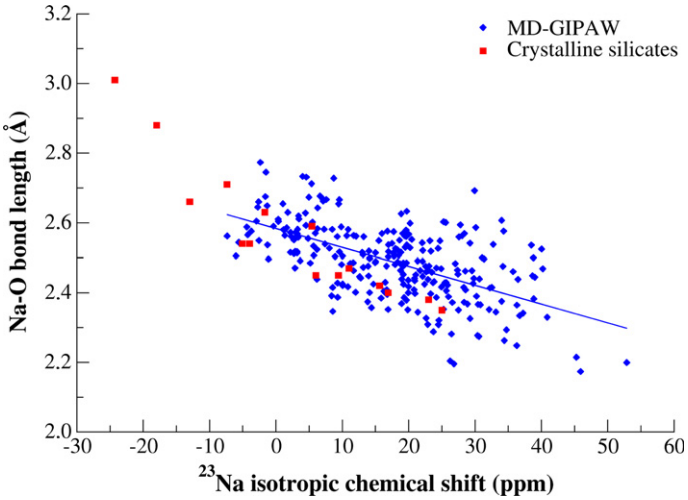

Fig. 3. Relations between ^{23}Na δ_{iso} MD-GIPAW calculated and Na–O bond length (diamonds). Experimental data from previous relationship obtained on crystalline silicates compounds for ^{23}Na (from (Angeli et al., 2000a and references therein)) are reported (squares) The solid line is a linear fit of equation: $d(Na–O) = -0.0054.\delta_{iso} + 2.5835$.

Table 4
MD-GIPAW ^{23}Na NMR parameters with respect to its oxygen coordination number (CN_O) obtained using a Na–O cutoff distance of 3.2 Å (average values coming from the glass compositions of Table 2). Standard deviations (see text) are given in parentheses.

CN_O	^{23}Na δ_{iso} (ppm)	^{23}Na P_Q (MHz)[a]	Mean Na–O distance (Å)	Shortest Na–BO distance (Å)	Shortest Na–NBO distance (Å)
4	11.8 (13.8)	5.3 (1.6)	2.34 (0.19)	2.63 (0.28)	2.20 (0.06)
5	7.4 (10.8)	4.7 (1.6)	2.45 (0.25)	2.61 (0.82)	2.24 (0.07)
6	6.5 (11.2)	4.5 (1.7)	2.52 (0.29)	2.54 (0.25)	2.23 (0.06)
7	2.2 (12.2)	4.4 (1.6)	2.59 (0.30)	2.51 (0.23)	2.25 (0.10)
8	−0.6 (7.9)	5.3 (1.5)	2.68 (0.32)	2.52 (0.17)	2.30 (0.05)

[a] The quadrupolar coupling parameters are defined as $P_Q = C_Q\,(1+\eta^2/3)^{1/2}$.

experimental value for NSMo glass is 47%. This lower value may correspond to the transition of network-modifying sodium atoms to charge-compensating positions for $[MoO_4]^{2-}$ groups. This result complements recent ^{29}Si observations showing an increase in the most polymerized Q^n species when Mo is added (Caurant et al., 2010). As the Na–O bond distances are generally smaller when sodium is a network modifier than a charge compensator (Angeli et al., 2000a), adding Mo in the glass should increase the mean Na–O distances and thus diminish ^{23}Na δ_{iso}. The differences between these shifts for NSMo and NS1 (Table 3) are probably at least partly related to this effect, the other part being possibly related to the lower Na concentration in NSMo.

4.2.2. Si–O–Si bond angles

The dependence of the isotropic chemical shift of ^{29}Si with its local environment is well established from empirical relationships and theoretical approaches (Sherriff et al., 1991; Engelhardt and Koller, 1994): linear correlations have been reported with the Si–O bond length (Smith et al., 1983; Grimmer, 1985) as well as the bond angles of the silicate network (Mägi et al., 1984; Radeglia and Engelhardt, 1985; Pettifer et al., 1988; Gladden et al., 1986; Bull et al., 2000; Mauri et al., 2000). The latter dependence is also observed for the MD-GIPAW data as shown in Fig. 4 (Left panel). Here, in order to *invert* our ^{29}Si MAS NMR data, we have extended the method introduced by (Mauri et al., 2000) which primarily aimed at extracting an estimation of the mean and standard deviation of the bond angle distribution from the ^{29}Si NMR spectrum. In our case, we applied this procedure to each Q^n species NMR line, so that we extracted the same information but for the Q^n-centered bond angle distribution (i.e. the bond angle distribution seen by each Q^n unit).

The relationship between ^{29}Si δ_{iso} of a Q^n unit and the bond angles of the n Si tetrahedral linkages is parameterized as follows:

$$\delta_{iso} = \frac{1}{n}\sum_{k=1}^{k=n} F(\theta_k) \text{with} F(\theta) = a_0 + a_1 + cos\,\theta + a_2 cos\,2\theta \tag{5}$$

The values of the a_i parameters were obtained from a least-square minimization analysis of the MD-GIPAW data, independently for each Q^n species. As shown in Fig. 4 (right panel), δ_{iso} can indeed be predicted with accuracy (see Table 5) of about 2 ppm. From the linear regressions plotted in Fig. 4 (left panel), the accuracy of the angle determination can be estimated to be in the range 2–4°.

With the help of Eq. (5), each ^{29}Si Q^n MAS NMR peak (which is in fact a distribution of δ_{iso}) can then be fitted with

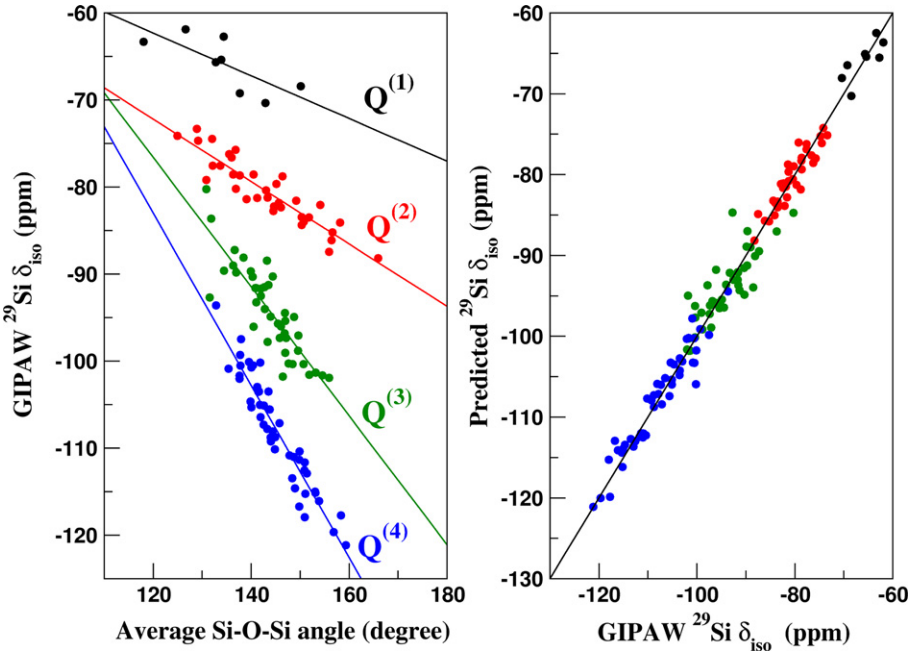

Fig. 4. (Left panel) Variation of the MD-GIPAW ^{29}Si isotropic chemical shift as a function of the mean Si–O–Si bond angle. Solid lines are linear regressions. (Right panel) Predicted (Eq. 5) versus MD-GIPAW ^{29}Si isotropic chemical shifts.

Table 5
Parameters used in the relationship between ^{29}Si δ_{iso} Q^n unit and the n bond angles ($\delta_{iso} = \frac{1}{n}\sum_{k=1}^{k=n} F(\theta_k)$ with $F(\theta) = a_0 + a_1\cos\theta + a_2\cos 2\theta$) and the resulting statistics of the Si–O–Si bong angle distribution as extracted from the fit of the ^{29}Si MAS NMR spectra. Standard deviations (see text) are given in parentheses.

Si units	a_0	a_1	a_2	Error std. dev.	Si–O–Si bond angle (°)			
					NS1	NSMo	NS3	SiO_2
Q^4	−18.86	110.97	1.78	1.8 ppm			141.6	146.0
							(8.2)	(8.2)
Q^3	−106.32	−26.25	−30.71	2.2 ppm	132.4	133.2	141.8	
					(10.4)	(10.4)	(9.3)	
Q^2	−90.78	−19.00	−17.66	1.5 ppm	134.1	134.7		
					(11.3)	(8.7)		
⟨Si–O–Si⟩ mean bond angle (°)					133.2	133.5	141.7	146.0

an analytical model of bond angle distribution (here a normal distribution was chosen). From the latter, mean and standard deviation values can be estimated. The corresponding results are shown with the Si–O–Si bond angle values in Table 5, where a bond angle is given for each Q^n species. Finally, an overall mean Si–O–Si angle is calculated taking account of the proportion of Q^n and the number of Si–O–Si bonds in each Q^n species.

A mean Si–O–Si bond angle near 146° is obtained for vitreous silica with a downward shift as the alkali concentration increases, reaching 133° for a glass containing 43% Na_2O. X-ray diffraction and absorption data (Wright, 1994) place the most probable angle for pure silica between 144° (Mozzi and Warren, 1969), 147° (Poulsen et al., 1995), and 152° (da Silva et al., 1975), in good agreement with our findings. MD simulations reveal a slight decrease in the Si–O–Si angular value and distribution when sodium is added to silica (Meyer et al., 2004; Du and Cormack, 2004), although the angular variations between glass compositions are less prominent than those derived from our NMR observations. XANES data have also been used to infer a decrease of Si–Si distances (Henderson, 1995). This is consistent with our observations concerning the decreasing Si–O–Si angle (closer Si–Si distances) as Na concentration increases.

4.3. Oxygen-17 NMR

Figs. 1c and 5 compare ^{17}O MAS and MQMAS spectra, respectively, of the studied glasses. The difference of ionic character of the two species (Si–BO and Si–NBO) leads to a clear separation in C_Q dimension (Oldfield and Kirkpatrick, 1985). The simulated spectra have been generated using the 3D NMR parameter distributions accounting for correlation

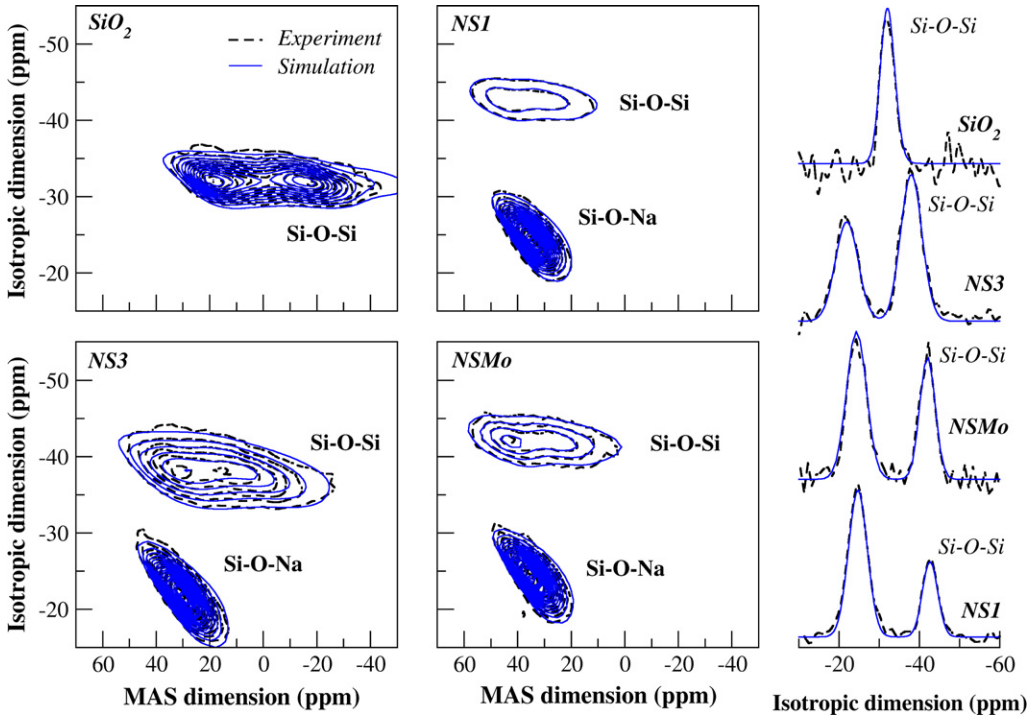

Fig. 5. Experimental and simulated ^{17}O MQMAS spectra and their projections on the isotropic dimension.

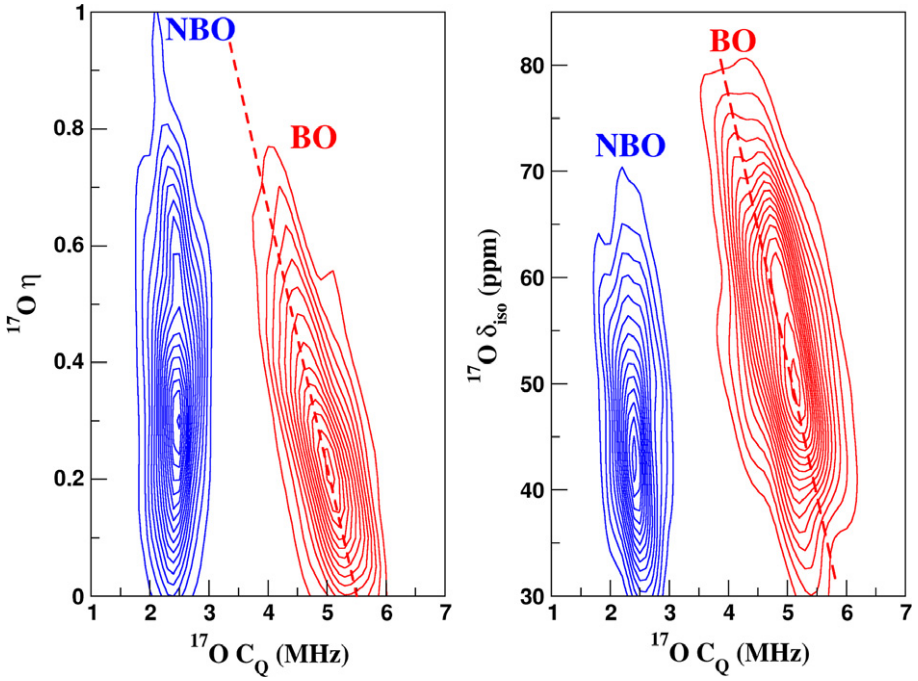

Fig. 6. Contour plots of the MD-GIPAW two-dimensional distributions $p(C_Q, \eta)$ and $p(C_Q, \delta_{iso})$ for ^{17}O. Dashed lines serve as guide for the eyes to visualize the correlation between the NMR parameters. Details on the deconvolution of the ^{17}O MQMAS spectrum are shown in Fig. 7 for one of the glass composition (NS3). For the extracted 3D NMR distribution, mean and standard deviations values for each parameter can then be calculated as reported in Table 3.

effects between the NMR parameters (see experimental section). The choice of such correlations is indeed corroborated both by the MD-GIPAW calculations as displayed in Fig. 6 and by the decrease of the mean squared error by about a factor 2 when compared to a non-correlated model (i.e. $a = 0$ in Eq. 3). The deconvolution of the ^{17}O MQMAS spectrum is

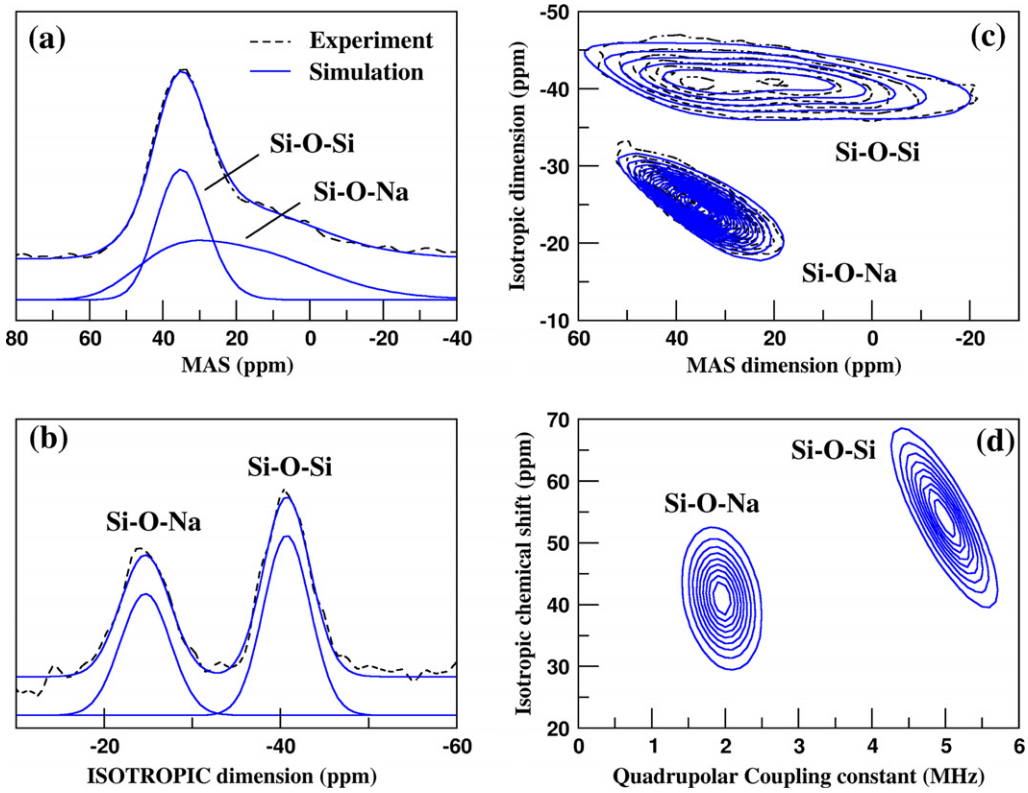

Fig. 7. Fit of the ^{17}O MQMAS spectrum of NS3 glass. (a) MAS and (b) projection on the isotropic dimension of the MQMAS spectrum. (c) Contour plots of the MQMAS experimental and simulated spectra and (d) the two-dimensional projection of the extracted NMR parameter distributions (δ_{iso} and C_Q).

detailed in Fig. 7 for one of the glass composition (NS3). To the best of our knowledge, this is the first time that such a good agreement has been obtained, better than our previous (uncorrelated model) approach (Angeli et al., 2008).

4.3.1. Si–O bond lengths

It has been reported that the ^{17}O δ_{iso} increases as a linear function of the Si–O bond distance in crystalline silicates (Ashbrook et al., 2001, 2002). Using the same approach as for ^{23}Na, the Si–O bond length can be estimated for our glass samples (Table 3) using either the MD-GIPAW correlation (Fig. 8a): $d(Si–O) = 0.00176\delta_{iso}(^{17}O) + 1.5357$, or from previous data on crystalline compounds: $d(Si–O) = 0.0025\delta_{iso}(^{17}O) + 1.4898$ (deduced from the data of Ashbrook et al., 2002). The comparison of bond lengths shows again a good agreement. For SiO_2 glass, the MD-GIPAW approach gives a slightly longer Si–O bond distance (1.600 Å) than the empirical relationship (1.582 Å). These values are consistent with that obtained by (Clark et al., 2004) in silica glass from the interpretation of ^{17}O DAS NMR spectra with a Si–O distance of 1.59 Å. The bond lengths increase when sodium is added, e.g. with a bond distance of 1.645 Å for NS1. For NS3 glass, our values are in agreement with neutron and X-ray diffraction which give a Si–O distance of 1.62 Å for a sodium silicate glass containing 30% of Na_2O (Fabian et al., 2007). It is worth noticing that the correlation between ^{17}O δ_{iso} and Si–O bond length only applies to bridging oxygens. Indeed, Fig. 8b displays the MD-GIPAW calculations for NBOs and implies that there is no clear relation between δ_{iso} and Si–NBO bond distance.

4.3.2. Molybdenum NMR signature

The molybdenum site (i.e. Mo–O) lies outside the area shown in the MQMAS spectra in Fig. 5. In Fig. 9a, an enlarged view of the ^{17}O MAS spectrum of the NSMo glass is shown and, for the first time, it is suggesting a contribution of the molybdenum site at about 510 ppm due to Na-compensated $[MoO_4]^{2-}$ groups. We have synthesized a Na_2MoO_4 crystalline phase enriched in ^{17}O (40%). For this phase, ^{17}O NMR GIPAW calculations were also done in order to localize the ^{17}O peak of Mo-O-Na contribution in our experimental data. This phase has already been recently studied by the GIPAW method (Cuny et al., 2009) where the ^{95}Mo NMR signature in alkaline and alkaline-earth oxides was investigated. The same parameters were used here. Comparison of the experimental NSMo glass spectrum with that of the simulation confirms the assignment to Na-compensated $[MoO_4]^{2-}$ groups in our Mo bearing glass (Fig. 9b). It is of note that the difference between the theoretical and experimental peak position (522 and 526 ppm respectively) is less than 5 ppm (about 1%), demonstrating the high accuracy of the GIPAW method. A second calculation has been performed on $CaMoO_4$ and the position of the Mo–O–Ca line was predicted to occur at about 590 ppm, confirming the high sensitivity of ^{17}O

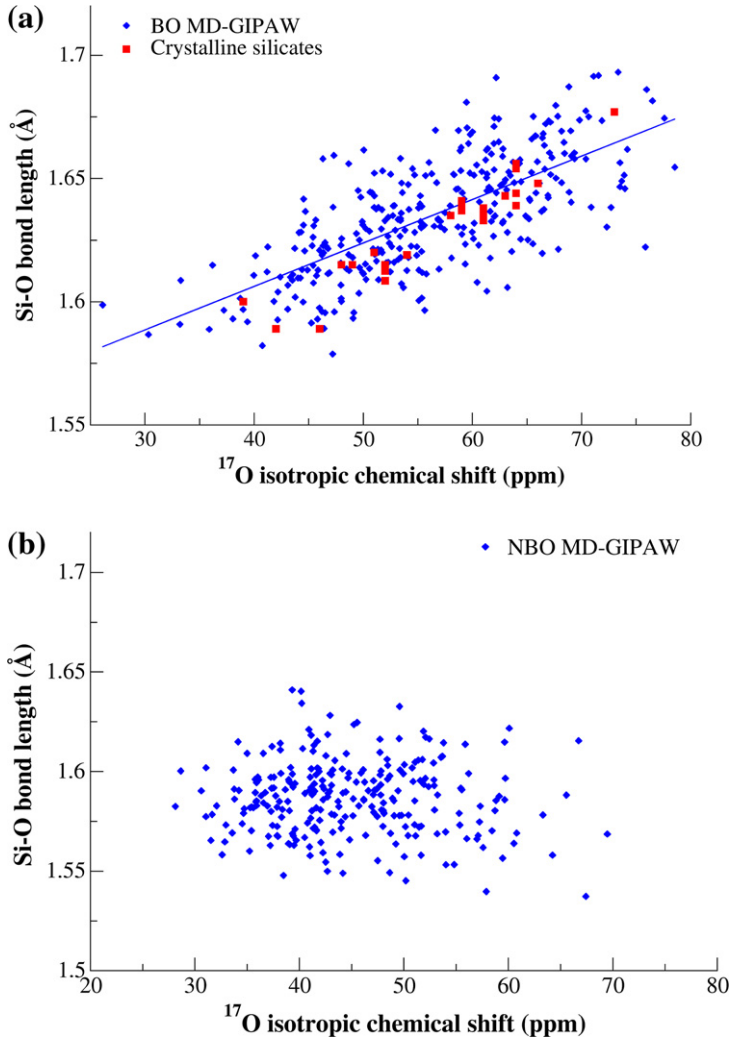

Fig. 8. Relations between ^{17}O δ_{iso} MD-GIPAW calculated and Si–O bond length (diamonds) for bridging oxygen (a) and non-bridging oxygen (b). Experimental data (squares) from previous relationships obtained on crystalline silicates compounds for ^{17}O (from (Ashbrook et al., 2002 and references therein)) are reported in (a). The solid line is a linear fit of equation: $d(Si–O) = 0.00176\delta_{iso}(^{17}O) + 1.5357$.

NMR to the change of cationic environment of MoO_4 units. Considering the width of the Mo–O–Na line (here 20 ppm), this opens up appealing new possibilities for investigating the Mo environment in glasses, especially for distinguishing and quantifying alkali and alkaline-earth molybdates sites.

4.3.3. Distribution of alkali ions

^{17}O MQMAS NMR spectra show the continuous shift of the sites with increasing Na concentration, and particularly that of the bridging Si–O–Si site (Fig. 5). This trend can be clearly observed from the two-dimensional projection of the extracted δ_{iso} and C_Q distributions (Fig. 10). The most broadly distributed line is that of the Si–O–Si site in the NS3 glass with 23% Na_2O. A small portion of this line is shared with the Si–O–Si line of the silica glass. This overlap can be attributed to the Q^4 species (37%) in NS3 glass. The extent of the C_Q distribution is then probably related to the extent of the Q^n distribution. Conversely, no overlapping is observed in the glass with the highest Na content (NS1) containing no Q^4 species; no residual contribution near the silica site corresponding to silica rich areas has been found. These findings suggest again a uniform distribution of alkali ions in the glass network.

The variations of the obtained mean δ_{iso} and C_Q versus the Na_2O proportion are shown in Fig. 11, and they are in good agreement with data recently reported by Lee and Stebbins (2009). However, we note that there are some small discrepancies between the two data sets; they can be ascribed to the fact that here we report accurate mean values (i.e. calculated from a NMR parameter distribution) whereas previous measurements where based on the peak positions (centers of gravity of each oxygen peak) in the isotropic dimension of the MQMAS spectrum. The sodium content in the NSMo glass was calculated removing the sodium involved in the formation of Na-compensated $[MoO_4]^{2-}$ groups. An almost perfect

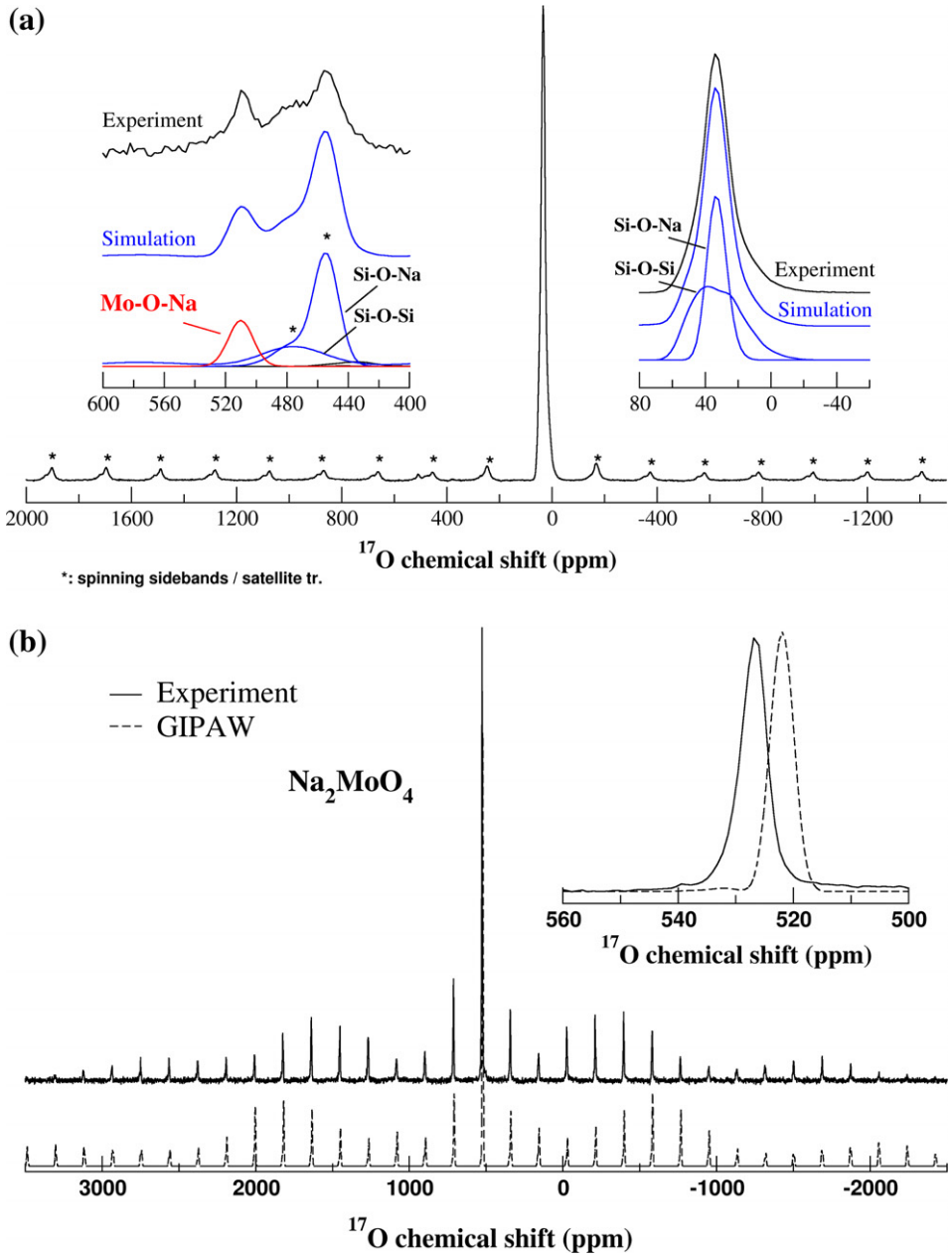

Fig. 9. (a) Enlarged views of the ^{17}O MAS NMR spectrum of NSMo glass showing the contribution of the molybdenum site and BO/NBO contributions (*: spinning sidebands). (b) Experimental (solid lines) and simulated (GIPAW, dashed lines) ^{17}O MAS NMR spectrum (insert: enlarged view) of Na_2MoO_4 crystalline phase (^{17}O enriched).

linear increase of δ_{iso} and decrease of C_Q for the BOs from SiO_2 to NS1 glass is observed. In contrast, the variations for the NBOs do not exhibit such an obvious trend. The δ_{iso} increase for the Si–BO bonds suggests some interactions between Na^+ ions and the oxygen atoms of the Si–O–Si bridges, in accordance with our ^{23}Na MAS NMR data. Moreover, we note that significant bonding of BO to modifiers has been recently suggested by MD (Mountjoy, 2007). As evidenced by the present MD-GIPAW calculations, increasing the number of Na indeed leads to a decrease of the Si–O–Si bond angle and lengthening of the Si–O bonds (Table 6). As experimentally observed, the calculated δ_{iso} presented the most pronounced variations, and this is clearly related here to direct interaction of Na with the BOs. One may explain this trend by the fact that the sodium attracts the oxygen atom, increasing the Si–O distances and decreasing the Si–O–Si bond angle. Concerning the NBOs, the data of Table 6 may be used to suggest that the increase of their δ_{iso} ($Q^3 \rightarrow Q^1$) can be related to an increase of the number of surrounding sodium atoms which leads to an increase of the Si–NBO distance. However, these changes for Si–NBO are difficult to discriminate as observed on Fig. 8b.

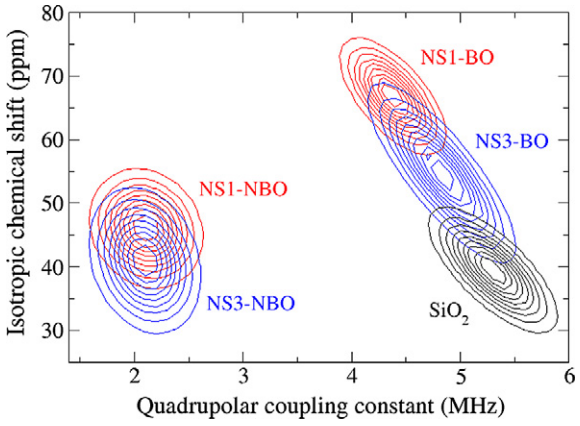

Fig. 10. Two-dimensional projection of the extracted ^{17}O NMR parameter distributions (δ_{iso} and C_Q) for bridging oxygen (BO) and non-bridging oxygen (NBO) of SiO_2 and sodium silicate glasses (NS1, NS3).

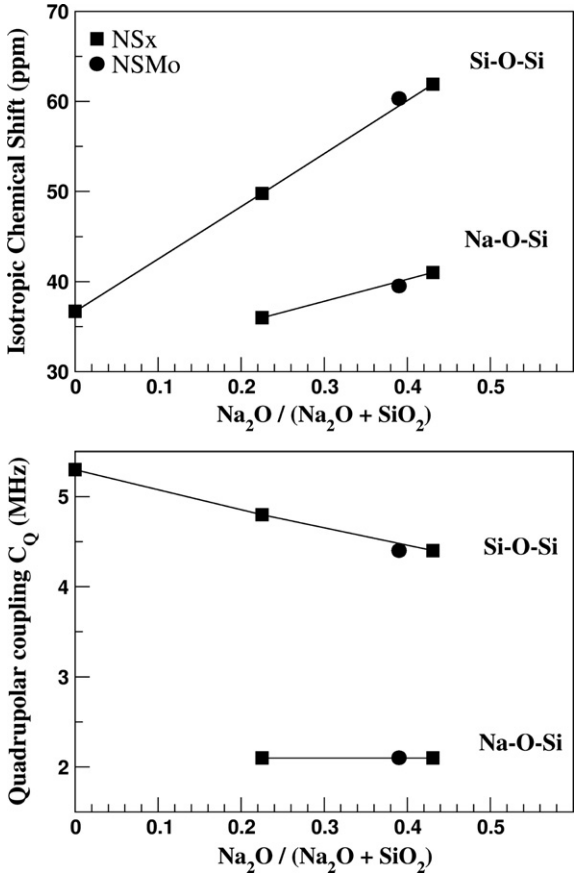

Fig. 11. Variations of the ^{17}O mean isotropic chemical shift and quadrupolar coupling parameter C_Q of the Si–O–Si and Na–O–Si oxygen-site for binary sodium silicate glass.

4.3.4. Si–O bond lengths and Si–O–Si bond angles

The ^{17}O C_Q can provide data on the topology of glass network. Based on the evolution of C_Q, as already noted by MD (Angeli et al., 2000b; Segall et al., 2002; Pedone et al., 2008), Lee and Stebbins (2009) reported a qualitative reduction in the Si–O–Si bond angle from ^{17}O NMR with increasing concentration of sodium. The dependence of the ^{17}O NMR quadrupolar parameters upon the Si–O–Si bond angle and Si–O bond distance has been extensively studied in literature with ab initio calculations on clusters (Kanzaki, 1998; Vermillion et al., 1998; Xue and Kanzaki, 1998, 1999, 2000; Clark et al., 2003, 2004). The MD-GIPAW data were analyzed with the help of classical relationships (Clark and Grandinetti, 2003, 2005). Concerning C_Q, we investigated two models:

$$C_Q(\theta,d) = A\left(\frac{1}{2}+\frac{\cos\theta}{\cos\theta-1}\right)^{\alpha} + m_d(d-d_0) \quad (6)$$

$$C_Q(\theta) = A\left(\frac{1}{2}+\frac{\cos\theta}{\cos\theta-1}\right)^{\alpha} + \Delta C_Q \quad (7)$$

where θ = Si–O–Si and d=Si–O. In contrast to a previous study (Ispas et al., 2010) it was found that including the d-dependence (Eq. 6) does not improve the precision. For both models the predicted C_Q values were found to agree with the MD-GIPAW values to within 0.31 MHz (standard deviations). This may be explained by the difference in glass compositions. Indeed, as a consequence of the higher sodium content in our glasses, BOs have stronger interactions with sodium atoms so that the latter contribute to the Electric Field Gradient (EFG). A more detailed analysis being out of the scope of the present work, the second model Eq. (7) was used to obtain a simple estimation of the bond angle distribution. A least-square error minimization of the MD-GIPAW data has yielded the parameters $A = 5.58$ MHz, $\alpha = 1.725$, $\Delta C_Q = -0.146$ MHz.

Concerning the asymmetrical parameter, the following model was used

$$\eta_Q(\theta) = B\left(\frac{1}{2}-\frac{\cos\theta}{\cos\theta-1}\right)^{\beta} + \Delta\eta_Q \quad (8)$$

The obtained parameters were $B = 3.98$, $\beta = 1.095$ and $\Delta\eta_Q = 0.103$; the precision was 0.11 (0.13 when omitting the second constant term in the right hand side of Eq. (8)). Fig. 12 reports the correlation between the ^{17}O quadrupolar parameters (C_Q and η_Q) and the Si–O–Si bond angle. With the help of the above equations and thanks to the fact that C_Q and η_Q distributions could be extracted from the ^{17}O MQMAS, statistics of bond angle distribution could be estimated and the corresponding results are reported in Table 7. Incorporating a variation of the ΔCq term into Eq. (7) with respect to the number of coordinating sodium was used to improve the Si–O–Si bond angle determination. For SiO_2 glass, the resulting mean bond angle value is 152°, slightly higher than the value around 147° previously obtained (Clark et al., 2004; Charpentier et al., 2009). For glasses with higher Na content (NS1 and NSMo), a narrower distribution than for vitreous silica is observed, with a smaller mean bond angle. Analysis of the quadrupolar coupling parameter distribution obtained by ^{17}O DAS NMR (Farnan et al., 1992) for a potassium silicate glass yielded angular distributions extending from 135° to 156° with a maximum at 143°. Authors compared their data with XRD data (Mozzi and Warren, 1969), revealing a slightly narrower distribution and a smaller

Table 6
MD-GIPAW statistics of bridging (up) and non-bridging (down) ^{17}O NMR parameters and structural factors with respect to sodium coordination numbers (CN_{Na}) obtained with a O-Na cutoff distance of 3.2 Å (average values coming from the glass compositions of Table 2). The standard deviations (see text) are given in parentheses.

CN_{Na}	Si–O–Si (degree)	O_{BO}–Si (Å)	^{17}O δ_{iso} (ppm)	^{17}O C_Q (MHz)	^{17}O η_Q	O_{BO}–Na (Å)	Shortest O_{BO}–Na (Å)
0	145.4	1.608	48.8	5.1	0.22		
	(11.1)	(0.018)	(8.5)	(0.4)	(0.13)		
1	146.2	1.629	54.1	4.9	0.29	2.62	2.62
	(13.1)	(0.026)	(7.6)	(0.4)	(0.18)	(0.27)	(0.27)
2	143.7	1.647	60.3	4.8	0.31	2.66	2.47
	(12.8)	(0.030)	(7.7)	(0.5)	(0.19)	(0.17)	(0.19)
3	143.1	1.661	64.2	4.8	0.33	2.74	2.46
	(13.8)	(0.030)	(7.3)	(0.5)	(0.18)	(0.12)	(0.15)
	^{17}O δ_{iso} (ppm)	^{17}O C_Q (MHz)	$^{17}O\eta_Q$	O_{NBO}-Si (Å)	CN_{Na}	O_{NBO}-Na (Å)	Shortest O_{NBO}-Na (Å)
NBO-Q^3	42.7	2.4	0.35	1.570	3.7	2.44	2.23
	(8.2)	(0.2)	(0.20)	(0.012)	(0.8)	(0.26)	(0.07)
NBO-Q^2	45.4	2.4	0.35	1.589	3.9	2.41	2.22
	(7.2)	(0.3)	(0.17)	(0.012)	(0.8)	(0.23)	(0.07)
NBO-Q^1	47.6	2.4	0.41	1.612	4.3	2.42	2.23
	(8.0)	(0.3)	(0.19)	(0.012)	(0.7)	(0.23)	(0.07)

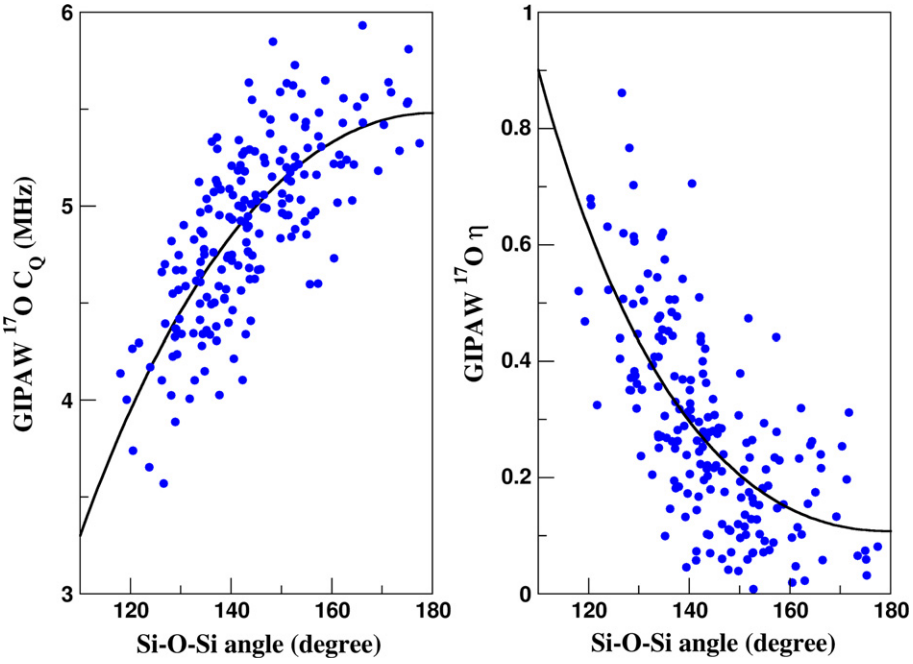

Fig. 12. ^{17}O NMR quadrupolar parameters C_Q (left) and η_Q (right) of bridging oxygen versus the Si–O–Si bond angle. Solid lines correspond to Eq. (7) and (8).

Table 7
Si–O–Si bond angle (and standard deviation, see text) calculated from C_Q and η_Q ^{17}O distributions

Glass	<Si–O–Si> mean bond angle (°)	
	from ^{17}O C_Q distribution	from ^{17}O η_Q distribution
NS3	142.7 (12.4)	135.1 (12.7)
NSMo	130.6 (5.1)	131.8 (8.6)
NS1	129.2 (5.5)	131.1 (8.6)
SiO_2	152.0 (13.2)	

mean bond angle than for vitreous silica, which is in agreement with our results for sodium silicate glasses. The angular distribution for the glass with lower sodium content (NS3) is similar to SiO_2, probably due to a higher Q^4 proportion compared with other sodium silicate glasses.

These findings suggest that ^{17}O quadrupolar NMR parameters are more difficult to analyze in terms of Si–O–Si and Si–O distance only, mainly because of the stronger interaction of Na with BO. Additionally, the ^{17}O relationships derived from sodium-bearing glasses are not directly

transferable to sodium free systems. Clearly, better functional accounting for Na interaction with BOs is needed but advanced NMR techniques probing Na–O environments would certainly be required. However, for all Q^n species, ^{29}Si δ_{iso} has been correlated to the Si–O–Si bond angle, resulting in a satisfactory agreement with the ^{17}O approach.

5. CONCLUSION

Comprehensive modeling of ^{17}O MQMAS spectra has allowed the extraction of the NMR parameters and thus opens the way to quantitative structural analysis of the data. In this work, classical MD simulations have been combined with first-principles NMR calculations in order to get more insights into the interpretation of the observed variations. It has been shown that ^{17}O quadrupolar NMR parameters are more difficult to analyze in terms of Si–O–Si and Si–O distance only, mainly because of the stronger interaction of Na with BO, strongly influencing its isotropic chemical shift. However, for all Q^n species, ^{29}Si isotropic chemical shift can be well correlated to the Si–O–Si bond angle. Thus, in good agreement with the ^{17}O spectra, the mean Si–O–Si bond angle decreases as the alkali concentration increases. The Si–O bond distance increases and the sodium atoms move closer to the oxygen atoms.

As observed from ^{23}Na and ^{17}O NMR, sodium cations have in their local environment both NBOs and BOs. Moreover, our findings suggest that ^{17}O NMR signatures as observed in vitreous silica (representative of fully polymerized regions), are definitely not observed in spectra of sodium silica glasses. In the same way, the NMR signature of BOs continuously shifts upon addition of sodium. According to our calculations, this can be explained by a decrease of the Si–O–Si bond angle, which only occurs when sodium atoms get closer to the oxygen atoms of the Si–O–Si linkage. The present data are therefore in favor of a homogeneous distribution of Na around both oxygen species (BO and NBO) in the silicate network for our glass compositions.

The presence of less than 1 mol% MoO_3 is sufficient to cause a 3% drop in the number of non-bridging oxygen atoms and clearly shows the influence of MoO_3 on glass structure based on the increase of the polymerization. The identification of the sodium molybdate site by ^{17}O NMR confirms the possibility of characterizing different possible molybdenum environments. The present data shows the high similarity of the environment of Mo in crystalline Na_2MoO_4 to that in sodium silicate glass, as supported by very close ^{17}O isotropic chemical shift. This opens new possibilities for investigating the Mo environment in glass, especially for distinguishing and quantifying alkali and alkaline-earth molybdate sites in more complex glasses.

Finally, our quantitative approach provides both the distribution and mean angular values, highlighting its potential for assessing the degree of disorder in the glass. It provides an overview that tallies with the data obtained for each nucleus, giving the bond distance and angle distributions as well as the overall distribution of alkali ions in the glass network. Given the importance of oxygen in a wide range of materials, the present approach represents a major step toward the emergence of new first-principles NMR based modeling techniques of glass.

ACKNOWLEDGEMENTS

This work was granted access to the HPC resources of CCRT under the allocation 2010-t20100096303 made by GENCI (Grand Equipement National de Calcul Intensif). The authors are grateful to three anonymous reviewers and to Associate Editor Michael Toplis for helpful comments.

REFERENCES

Advocat T., Jollivet P., Crovisier J. L. and Del Nero M. (2001) Long-term alteration mechanisms in water for SON68 radioactive borosilicate glass. *J. Nucl. Mater.* **298**(1–2), 55–62.

Angeli F., Charpentier T., Faucon P. and Petit J.-C. (1999) Structural characterization of glass from the inversion of ^{23}Na and ^{27}Al 3Q-MAS NMR spectra. *J. Phys. Chem. B* **103**(47), 10356–10364.

Angeli F., Charpentier T., Gaillard M. and Jollivet P. (2007) Contribution of ^{43}Ca MAS NMR for probing the structural configuration of calcium in glass. *Chem. Phys. Lett.* **440**(4–6), 324–328.

Angeli F., Charpentier T., Gaillard M. and Jollivet P. (2008) Influence of zirconium on the structure of pristine and leached soda-lime borosilicate glasses: towards a quantitative approach by ^{17}O MQMAS NMR. *J. Non-Cryst. Solids* **354**, 3713–3722.

Angeli F., Delaye J.-M., Charpentier T., Faucon P., Petit J.-C. and Ghaleb D. (2000a) Influence of glass chemical composition on the Na–O bond distance. a ^{23}Na 3Q-MAS NMR and molecular dynamics study. *J. Non-Cryst. Solids* **276**(1–3), 132–144.

Angeli F., Delaye J.-M., Charpentier T., Petit J.-C. and Ghaleb D. (2000b) Investigation of Al–O–Si bond angle in glass by ^{27}Al 3Q-MAS NMR and molecular dynamics. *Chem. Phys. Lett.* **320**(5–6), 681–687.

Ashbrook S. E., Berry A. J. and Wimperis S. (2001) O-17 multiple-quantum MAS NMR study of high-pressure hydrous magnesium silicates. *J. Am. Chem. Soc.* **123**(26), 6360–6366.

Ashbrook S. E., Berry A. J. and Wimperis S. (2002) O-17 multiple-quantum MAS NMR study of pyroxene. *J. Phys. Chem. B.* **106**(4), 773–778.

Bull L. M., Bussemer B., Anupold T., Reinhold A., Samoson A., Sauer J., Cheetham A. K. and Dupree R. (2000) A high-resolution ^{17}O and ^{29}Si NMR study of zeolite siliceous ferrierite and ab initio calculations of NMR parameters. *J. Am. Chem. Soc.* **122**, 4948–4958.

Calas G., Le Grand M., Galoisy L. and Ghaleb D. (2003) Structural role of molybdenum in nuclear glasses: an EXAFS study. *J. Nucl. Mater.* **322**(1), 15–20.

Carré A., Horbach J., Ispas S. and Kob W. (2008) New fitting scheme to obtain effective potential from Car-Parrinello molecular-dynamics simulations: application to silica. *Europhys. Lett.* **82**(17001), 1–6.

Caurant D., Majérus O., Fadel E., Lenoir M., Gervais C. and Pinet O. (2007) Effect of molybdenum on the structure and on the crystallization of SiO_2–Na_2O–CaO–B_2O_3 glasses. *J. Am. Ceram. Soc.* **90**(3), 774–783.

Caurant D., Majérus O., Fadel E., Quintas A., Gervais C., Charpentier T. and Neuville D. (2010) Structural investigations of borosilicate glasses containing MoO_3 by MAS NMR and Raman spectroscopies. *J. Nucl. Mater.* **396**(1), 94–101.

Charpentier T., Ispas S., Profeta M. and Mauri F. (2004) First-principles calculation of O-17, Si-29, and Na-23 NMR spectra

of sodium silicate crystals and glasses. *J. Phys. Chem. B.* **108**(13), 4147–4161.

Charpentier T., Kroll P. and Mauri F. (2009) First-principles nuclear magnetic resonance structural analysis of vitreous silica. *J. Phys. Chem. C.* **113**(18), 7917–7929.

Clark T. M. and Grandinetti P. J. (2003) Dependence of bridging oxygen O-17 quadrupolar coupling parameters on Si–O distance and Si–O–Si angle. *J. Phys. Condens. Matter.* **15**(31), 2387–2395.

Clark T. M. and Grandinetti P. J. (2005) Calculation of bridging oxygen O-17 quadrupolar coupling parameters in alkali silicates: a combined ab initio investigation. *Solid State NMR* **27**(4), 233–241.

Clark T. M., Grandinetti P. J., Florian P. and Stebbins J. F. (2004) Correlated structural distributions in silica glass. *Phys. Rev. B* **70**(6), 202.

Clark S. J., Segall M. D., Pickard C. J., Hasnip P. J., Probert M. J., Refson K. and Payne M. C. (2005) First principles methods using CASTEP. *Z. Kristallogr.* **220**(5–6), 567–570.

Cuny J., Furet E., Gautier R., Le Pollès L., Pickar C. J. and d'Espinose de Lacaillerie J.-B. (2009) Density functional theory calculations of Mo-95 NMR parameters in solid-state compounds. *Chem. Phys. Chem.* **10**(18), 3320–3329.

Czjzek G., Fink J., Götz F., Schmidt H., Coey J. M. D., Rebouillat J. P. and Liénard A. (1981) Atomic coordination and the distribution of electric field gradients in amorphous solids. *Phys. Rev B* **23**, 2513–2530.

da Silva J. R. G., Pinatti D. G., Anderson C. E. and Rudee M. L. (1975) Refinement of structure of vitreous silica. *Philos. Mag.* **31**(3), 713–717.

Du J. and Cormack A. N. (2004) The medium range structure of sodium silicate glasses: a molecular dynamics simulation. *J. Non-Cryst. Solids* **349**, 66–79.

Emerson J. F., Stallworth P. E. and Bray P. J. (1989) High-field ^{29}Si NMR studies of alkali silicate glasses, *J. Non-Cryst. Solids* **113**, 253–259.

Engelhardt G. and Koller H. (1994) *NMR Basic Principles and Progress 31, 1*. Springer-Verlag, Berlin.

Fabian M., Jovari P., Svab E., Meszaros G., Proffen T. and Veress E. (2007) Network structure of 0.7SiO(2)–0.3Na(2)O glass from neutron and X-ray diffraction and RMC modeling. *J. Phys.: Condens Matter* **19**(33), 335209.

Farges F., Siewert R., Brown E., Guesdon A. and Morin G. (2006) Structural environments around molybdenum in silicate glasses and melts I. Influence of composition and oxygen fugacity on the local structure of molybdenum. *Can. Miner.* **44**, 731–753.

Farnan I., Grandinetti P. J., Baltisberger J. H., Stebbins J. F., Werner U., Eastman M. A. and Pines A. (1992) Quantification of the disorder in network-modified silicate glasses. *Nature* **358**, 31–35.

Forler N., Vasconcelos F., Cristol S., Paul J. F., Montagne L., Charpentier T., Mauri F. and Delevoye L. (2010) New insights into oxygen environments generated during phosphate glass alteration: a combined 17O MAS and MQMAS NMR and first principles calculations study. *Phys. Chem. Chem. Phys.* **12**, 9053.

Gaskell P. H., Eckersley M. C., Barnes A. C. and Chieux P. (1991) Medium-range order in the cation distribution of a calcium silicate glass. *Nature* **350**, 675–677.

Gee B., Janssen M. and Eckert H. (1997) Local cation environments in mixed alkali silicate glasses studied by multinuclear single and double resonance magic-angle spinning NMR. *J. Non-Cryst. Solids* **215**, 41–50.

George A. M. and Stebbins J. F. (1995) High temperature Na-23 MAS NMR data for albite – comparison to chemical shift models. *Am. Miner.* **80**(9–10), 878–884.

Giacomazzi L., Umari P. and Pasquarello A. (2009) Medium-range structure of vitreous SiO_2 obtained through first-principles investigation of vibrational spectra. *Phys. Rev. B* **79**, 49.

Giannozzi P. (2009) QUANTUM ESPRESSO: a modular and open-source software project for quantum simulations of materials, *J. Phys. Condens. Matter* **21**, 39 (http://www.quantum-espresso.org).

Gladden L. F., Carpenter T. A. and Elliot S. R. (1986) Si-29 MAS NMR studies of the spin lattice relaxation time and bond angle distribution in vitreous silica. *Philos. Mag. B* **53**(4), 81–87.

Greaves G. N. (1985) EXAFS and the structure of glass. *J. Non-Cryst. Solids* **71**(1–3), 203–217.

Greaves G. N. (1989) EXAFS, glass structure and diffusion. *Philos. Mag. B* **60**(6), 793–800.

Grimmer A. R. (1985) Correlation between individual Si–O bond lengths and the principal values of the ^{29}Si chemical shift tensor in solid silicates. *Chem. Phys. Lett.* **119**(5), 416–420.

Henderson G. S. (1995) A Si K-edge EXAFS/XANES study of sodium–silicate glasses. *J. Non-Cryst. Solids* **183**(1–2), 43–50.

Horbach J., Kob W. and Binder K. (2002) Dynamics of sodium in sodium disilicate: channel relaxation and sodium diffusion. *Phys. Rev. B* **88**(12), 125502.

Ispas S., Charpentier T., Mauri F. and Neuville D. R. (2010) Structural properties of lithium and sodium tetrasilicate glasses: molecular dynamics simulations versus NMR experimental and first-principles data. *Solid State Sci.* **12**(2), 183.

Kargl F., Meyer A., Koza M. M. and Schober H. (2006) Formation of channels for fast-ion diffusion in alkali silicate melts: a quasielastic neutron scattering study. *Phys. Rev. B* **74**(1), 014304.

Kroeker S., Farnan I., Schuller S. and Advocat T. (2009) Mo-95 NMR study of crystallization in model nuclear waste glasses. *Scientific Basis Nuclear Waste Manage. XXXII* **1124**, 153–159.

Larsen F. H. and Farnan I. (2002) Si-29 and O-17 (Q)CPMG-MAS solid-state NMR experiments as an optimum approach for half-integer nuclei having long T-1 relaxation times. *Chem. Phys. Lett.* **357**(5–6), 403–408.

Lee S. K. and Stebbins J. F. (2003) The distribution of sodium ions in aluminosilicate glasses: a high-field Na-23 MAS and 3Q MAS NMR study. *Geochim. Cosmochim. Acta* **67**(9), 1699–1709.

Lee S. K. and Stebbins J. F. (2009) Effects of the degree of polymerization on the structure of sodium silicate and aluminosilicate glasses and melts: an O-17 NMR study. *Geochim. Cosmochim. Acta* **73**(4), 1109–1119.

Maekawa H., Maekawa T., Kawamura K. and Yokokawa T. (1991) The structural groups of alkali silicate glasses determined from ^{29}Si MAS-NMR. *J. Non-Cryst. Solids* **127**, 53–64.

Maekawa H., Nakao T., Shimokawa S. and Yokokawa T. (1997) Coordination of sodium ions in $NaAlO_2$–SiO_2 melts: A high temperature Na-23 NMR study. *Phys. Chem. Min.* **24**(1), 53–65.

Mägi M., Lippmaa E., Samoson A., Engelhardt G. and Grimmer A.-R. (1984) Solid state high resolution Si-29 chemical shifts in silicates. *J. Phys. Chem.* **88**(8), 1518–1522.

Mauri F., Pasquarello A., Pfrommer B. G., Yoon Y. G. and Louie S. G. (2000) Si–O–Si bond-angle distribution in vitreous silica from first-principles Si-29 NMR analysis. *Phys. Rev. B* **62**(8), R4786–R4789.

Meyer A., Horbach J., Kob W., Kargl F. and Schober H. (2004) Channel formation and intermediate range order in sodium silicate melts and glasses. *Phys. Rev. Lett.* **93**(2), 027801–027811.

Mountjoy G. (2007) The local atomic environment of oxygen in silicate glasses from molecular dynamics. *J. Non-Cryst. Solids* **353**(18–21), 1849–1853.

Mozzi R. L. and Warren B. E. (1969) The structure of vitreous silica. *J. Appl. Cryst* **2**, 164–172.

Neuefeind J. and Liss K. D. (1996) Bond angle distribution in amorphous germania and silica. *Ber. Bunsen-Ges.* **100**(8), 1341–1349.

Neuville D. R., Cormier L. and Massiot D. (2004) Al environment in tectosilicate and peraluminous glasses: a Al-27 MQ-MAS NMR, Raman, and XANES investigation. *Geochim. Cosmochim. Acta* **68**(24), 5071–5079.

Oldfield E. and Kirkpatrick R. J. (1985) High-resolution nuclear magnetic resonance of inorganic solids. *Science* **227**(4694), 1537–1544.

Pedone A., Charpentier T., Malavasi G. and Menziani M. C. (2010a) New Insights into the atomic structure of 45S5 bioglass by means of solid-state NMR spectroscopy and accurate first-principles simulations. *Chem. Mater.* **22**, 5644–5652.

Pedone A., Charpentier T. and Menziani M. C. (2010b) Multinuclear NMR of $CaSiO_3$ glass: simulation from first-principles. *Phys. Chem. Chem. Phys.* **12**(23), 6054–6066.

Pedone A., Malavasi G., Cormack A. N., Segre U. and Menziani M. C. (2008) Elastic and dynamical properties of alkali-silicate glasses from computer simulations techniques. *Theor. Chem. Acc.* **120**(4–6), 557–564.

Pedone A., Malavasi G., Menziani M. C., Cormack A. N. and Segre U. (2006) A new self-consistent empirical interatomic potential model for oxides, silicates, and silica-based glasses. *J. Phys. Chem. B* **110**(24), 11780–11795.

Perdew J. P., Burke K. and Ernzerhof M. (1996) Generalized gradient approximation made simple. *Phys. Rev. Lett.* **77**(18), 3865–3898.

Pettifer R. F., Dupree R., Farnan I. and Sternberg U. (1988) NMR determinations of Si–O–Si bond angle distributions in silica. *J. Non-Cryst. Solids* **106**(1–3), 408–412.

Pickard C. J. and Mauri F. (2001) All-electron magnetic response with pseudopotentials: NMR chemical shifts. *Phys. Rev. B* **63**(24), 245101.

Pinet O., Grandjean A., Frugier P., Rabiller H. and Poissonet S. (2006) Leaching behavior of a polyphase glass-ceramic containment matrix. *J. Non-Cryst. Solids* **352**(28–29), 3095–3102.

Poulsen H. F., Neuefeind J., Neumann H. B., Schneider J. R. and Zeidler M. D. (1995) Amorphous silica studied by high-energy X-ray diffraction. *J. Non-Cryst. Solids* **188**(1–2), 63–74.

Profeta M., Mauri F. and Pickard C. J. (2003) Accurate first principles prediction of O-17 NMR parameters in SiO_2: assignment of the zeolite ferrierite spectrum. *J. Am. Chem. Soc.* **125**(2), 541–548.

Radeglia R. and Engelhardt G. (1985) Correlation of Si–O–T (T = Si or Al)–angles and ^{29}Si NMR chemical shifts in silicate and aluminosilicates. *Chem. Phys. Lett.* **114**, 28–30.

Rossano S., Mauri F., Pickard C. J. and Farnan I. (2005) First-principles calculation of O-17 and Mg-25 NMR shieldings in MgO at finite temperature: Rovibrational effect in solids. *J. Phys. Chem. B.* **109**(15), 7245–7250.

Schneider E., Stebbins J. F. and Pines A. (1987) Speciation and local structure in alkali and alkaline earth silicate glasses: constraints from ^{29}Si NMR spectroscopy. *J. Non-Cryst. Solids* **89**, 371–383.

Segall M. D., Lindan P. J. D., Probert M. J., Pickard C. J., Hasnip P. J., Clark S. J. and Payne M. C. (2002) First-principles simulation: ideas, illustrations and the CASTEP code. *J. Phys.: Condens. Matter* **14**(11), 2712–2744.

Sherriff B. L., Grundy H. D. and Hartman J. S. (1991) The relationship between ^{29}Si MAS NMR chemical shift and silicate mineral structure. *Eur. J. Mineral.* **3**, 751–768.

Short R. J., Hand R. J., Hyatt N. C. and Möbus G. (2005) Environment and oxidation state of molybdenum in simulated high level nuclear waste glass compositions. *J. Nucl. Mater.* **340**(2–3), 179–186.

Smith W. and Forester T. R. (1996) DL_POLY_2.0: a general-purpose parallel molecular dynamics simulation package. *Mol. Graphics* **14**(3), 136–141.

Smith K. A., Kirkpatrick R. J., Oldfield E. and Henderson D. M. (1983) High resolution silicon-29 nuclear magnetic resonance spectroscopy of rock-forming silicates. *Am. Mineral.* **68**, 1206–1215.

Soleilhavoup A., Delaye J.-M., Angeli F., Caurant D. and Charpentier T. (2010) Contribution of first-principles calculations to multinuclear NMR analysis of borosilicate Glass (2010). *Magn. Res. Chem.* **48**(1), 159–170.

Stebbins J. F. (1998) Cation sites in mixed-alkali oxide glasses: correlations of NMR chemical shift data with site size and bond distance. *Sol. State Ion.* **112**(1–2), 137–141.

Vermillion K. E., Florian P. and Grandinetti P. (1998) Relationships between bridging oxygen O-17 quadrupolar coupling parameters and structure in alkali silicates. *J. Chem. Phys.* **108**(17), 7274–7285.

Wright A. C. (1994) Neutron scattering from vitreous silica. *J. Non-Cryst. Solids* **179**, 84–115.

Xue X. Y. and Kanzaki M. (1998) Correlations between Si-29, O-17, and H-1 NMR properties and local structures in silicates: an ab initio calculation. *Phys. Chem. Miner.* **26**(1), 14–30.

Xue X. Y. and Kanzaki M. (1999) NMR characteristics of possible oxygen sites in aluminosilicate glasses and melts: an ab initio study. *J. Phys. Chem. B* **103**(49), 10816–10830.

Xue X. Y. and Kanzaki M. (2000) An ab initio calculation of O-17 and Si-29 NMR parameters for SiO_2 polymorphs. *Solid State Nucl. Magn. Reson.* **16**(4), 245–259.

Xue X. Y. and Stebbins J. F. (1993) Na-23 NMR chemical shifts and local Na coordination environments in silicate crystals, melts and glasses. *Phys. Chem. Min.* **20**(5), 297–307.

Yates J. R., Pickard C. J. and Mauri F. (2007) Calculation of NMR chemical shifts for extended systems using ultrasoft pseudopotentials. *Phys. Rev. B* **76**(2), 024401.

Yuan X. and Cormack A. N. (2003) Si–O–Si bond angle and torsion angle distribution in vitreous silica and sodium silicate glasses. *J. Non-Cryst. Solids* **319**, 31–43.

Zachariasen W. H. (1932) The atomic arrangement in glass. *J. Chem. Soc.* **54**, 3841–3851.